Biosensors and Bioelectronics 172 (2021) 112774

Contents lists available at ScienceDirect

Biosensors and Bioelectronics

journal homepage: http://www.elsevier.com/locate/bios

Glial-fibrillary-acidic-protein (GFAP) biomarker detection in serum-matrix: Functionalization strategies and detection by an ultra-high-frequency surface-acoustic-wave (UHF-SAW) lab-on-chip.

M. Agostini [a,b], F. Amato [a], M.L. Vieri [a], G. Greco [a], I. Tonazzini [a], L. Baroncelli [c,d], M. Caleo [c,e], E. Vannini [c], M. Santi [a], G. Signore [a,f], M. Cecchini [a,b,*]

[a] NEST, Istituto Nanoscienze-CNR and Scuola Normale Superiore, Piazza San Silvestro 12, 56127, Pisa, Italy
[b] INTA srl, Intelligent Acoustics Systems, Via Nino Pisano 14, 56122, Pisa, Italy
[c] Institute of Neuroscience, National Research Council (CNR), via G. Moruzzi 1, 56124, Pisa, Italy
[d] Department of Developmental Neuroscience, IRCCS Stella Maris Foundation, viale del Tirreno 331, 56128, Pisa, Italy
[e] Department of Biomedical Sciences, University of Padua, via G. Colombo 3, 35121, Padua, Italy
[f] Fondazione Pisana per la Scienza, Via Ferruccio Giovannini 13, 56017, Pisa, Italy

ARTICLE INFO

Keywords:
Biosensor
Lab-on-chip
Quartz crystal microbalance (QCM)
Surface acoustic wave (SAW)
Glial fibrillary acidic protein (GFAP)
Brain damage
Point of care

ABSTRACT

Glial-fibrillary-acidic-protein (GFAP) has recently drawn significant attention from the clinical environment as a promising biomarker. The pathologies which can be linked to the presence of GFAP in blood severely affect the human central nervous system. These pathologies are glioblastoma multiforme (GBM), traumatic brain injuries (TBIs), multiple sclerosis (MS), intracerebral hemorrhage (ICH), and neuromyelitis optica (NMO). Here, we develop three different detection strategies for GFAP, among the most popular in the biosensing field and never examined side by side within the experimental frame. We compare their capability of detecting GFAP in a clean-buffer and serum-matrix by using gold-coated quartz-crystal-microbalance (QCM) sensors. All the three detection strategies are based on antibodies, and each of them focuses on a key aspect of the biosensing process. The first is based on a polyethylene glycol (PEG) chain for antifouling, the second on a protein-G linker for controlling antibody-orientation, and the third on antibody-splitting and direct surface immobilization for high-surface coverage. Then, we select the best-performing protocol and validate its detection performance with an ultra-high-frequency (UHF) surface-acoustic-wave (SAW) based lab-on-chip (LoC). GFAP successful detection is demonstrated in a clean-buffer and serum-matrix at a concentration of 35 pM. This GFAP level is compatible with clinical diagnostics. This result suggests the use of our technology for the realization of a point-of-care biosensing platform for the detection of multiple brain-pathology biomarkers.

1. Introduction

The glial-fibrillary-acidic-protein (GFAP) is a type III intermediate filament protein mainly expressed by astrocytes in the central nervous system (CNS). Together with other proteins, GFAP has a central role in the structure and function of the cell cytoskeleton, preserving its shape and mechanical properties ("UniProt database," 2020). Indeed, it is one of the most popular markers for labeling astrocytes in biochemical procedures (Preston et al., 2019). In the last years, GFAP has been put under the spotlight of the clinical environment as a promising biomarker for severe brain-related pathologies in humans. The presence of GFAP in circulating blood has been linked to glioblastoma multiforme (GBM) (Jung et al., 2007; Tichy et al., 2016), traumatic brain injuries (TBIs) (Frankel et al., 2019; Nylén et al., 2006; Vos et al., 2004; Yue et al., 2019), multiple sclerosis (MS) (Abdelhak et al., 2018; Axelsson et al., 2011), intracerebral hemorrhage (ICH) (Zhang et al., 2013), and neuromyelitis optica (NMO) (Takano et al., 2010). The interest in GFAP as a biomarker is related to two main aspects. First, the importance of the pathologies that could be addressed. TBIs, for example, affect several millions of people every year and are considered one of the heaviest burdens of national healthcare systems in developed countries (Humphreys et al., 2013; Taylor et al., 2017). Second, the possibility to detect this biomarker in circulating blood, avoiding invasive procedures such as cerebrospinal fluid collection. A serum biomarker could be critical for

* Corresponding author. NEST, Istituto Nanoscienze-CNR and Scuola Normale Superiore, Piazza San Silvestro 12, 56127, Pisa, Italy.
E-mail address: marco.cecchini@nano.cnr.it (M. Cecchini).

https://doi.org/10.1016/j.bios.2020.112774
Received 7 August 2020; Received in revised form 6 October 2020; Accepted 27 October 2020
Available online 31 October 2020

establishing diagnosis and follow-up of CT-occult TBIs and ICHs (Wang et al., 2018; Zhang et al., 2013), for GBM monitoring and surveillance of recurrence (Jung et al., 2007), for improving MS diagnosis and prediction of disease progression (Axelsson et al., 2011; Abdelhak et al., 2018).

In light of this, a growing number of works has been recently published involving the detection of GFAP. The common aim is to propose technologies suitable for point-of-care (PoC) diagnostics. Arya et al. (2013) in 2013 and Wang et al. (Wang, 2017) in 2017 proposed electrochemical sensors for GFAP. The first one was based on immobilized anti-GFAP antibodies, while the second one exploited the molecularly-imprinted-polymer (MIP) technology. The first work showed a limit of detection (LoD) of a few tens of fM, while the second of hundreds of pM, both using a solution of GFAP in clean-buffers. J. Song et al. (2017) in 2017 detected a few tens of pM of GFAP in clean-buffers by using an organic-field-effect-transistor (OFET) with polyethylene glycol (PEG) based functionalization. To the best of our knowledge, the only paper showing a device for the detection of GFAP in serum-matrix was published by Y. Ma et al. (2018) in 2018. Here, carbon dots (CDs) functionalized with antibodies were used to label GFAP; detection was achieved by fluorescence and reached an LoD of the order of pM.

In the context of label-free methods with electrical readout and on-chip sample manipulation, the Rayleigh surface acoustic wave (SAW) technology represents a very promising mean. SAWs are acoustic waves that travel along a piezoelectric crystal surface, which can interact with materials (such as a fluid) placed on their path. The SAW-chips are planar devices with electrical feeding and readout which can be fabricated by standard complementary-metal-oxide-semiconductor (CMOS) processes. SAWs can be used as sensors for detecting adhesion of molecules onto surfaces, and for manipulating fluids at the micrometer scale as well. Thus, these mechanical waves are ideal for realizing fully integrated LoCs. SAWs can couple with fluids and activate several microfluidic phenomena, such as mixing (Friend and Yeo, 2011; Greco et al., 2017b; Shilton et al., 2014), droplet actuation (Franke et al., 2009; Shilton et al., 2015; Travagliati et al., 2012), microparticle manipulation (Destgeer and Sung, 2015; Travagliati et al., 2014), nebulization and micropumping (Cecchini et al., 2008; Friend and Yeo, 2011), dynamic cell culturing (Greco et al, 2017a, 2018). In our previous works, we also showed that ultra-high-frequency (UHF) SAW acoustic resonators can be configured for biosensing applications in liquids (Agostini et al., 2018; M. Agostini et al., 2019), outperforming standard commercial gravimetric sensors in terms of LoD. In the last few years, we developed this ultrasensitive full-SAW LoC capable of manipulating fluids and detecting

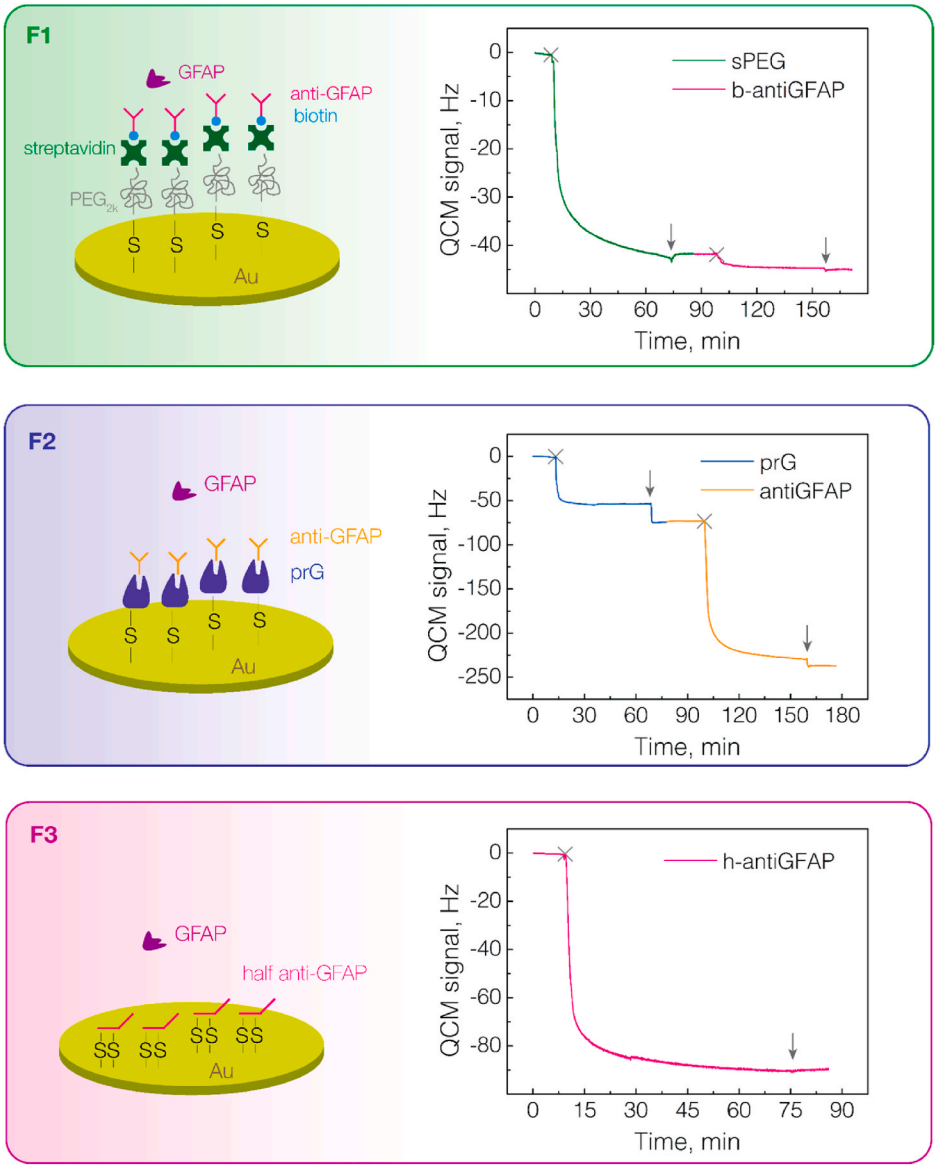

Fig. 1. The three functionalization strategies explored for GFAP detection with gold QCM sensors. F1 comprises an sPEG functionalization followed by the immobilization of the b-antiGFAP through the biotin-streptavidin binding. F2 comprises a functionalization with prG followed by the immobilization of the antiGFAP by the prG binding immunoglobulins. F3 makes use of the thiol-bridges of the reduced anti-GFAP. On the right-hand side, the binding kinetics during the different steps are shown. The cross symbol corresponds to solution injection, while the arrow to the rinsing with buffer.

sub-nM concentrations of proteins without signal amplification and labeling. This device, being miniaturized, fabricated with highly parallelizable processes, passive, with electrical-readout, is an ideal platform for the realization of a PoC instrument for GFAP detection.

In this work, we design and test three different and original functionalization strategies for GFAP detection. These functionalizations are based on the most popular methods in the biosensing field and never examined side by side within the experimental frame. All of them exploit anti-GFAP antibodies, differently linked to the sensor surface. The first strategy exploits a PEG layer for antifouling, the second the protein-G for antibody-orientation, and the third an antibody-splitting protocol for an enhanced surface-coverage. We first test these functionalizations both in clean-buffer and in serum-matrix with a quartz-crystal-microbalance (QCM). The QCM is a powerful tool for the investigation of surface chemistry, based on mass-detection with piezoelectric sensors. The ease of use of this instrument and its reliability are balanced by some limitations in terms of performance. Nonetheless, it allowed us to select the best-performing functionalization among the three strategies deployed before proceeding with a more sensitive detection platform. Indeed, we finally select the best performing strategy on QCM and apply it to the UHF-SAW LoC we previously developed. This very sensitive platform is used to validate the selected detection strategy with clinically relevant GFAP concentrations in clean-buffer and serum-matrix.

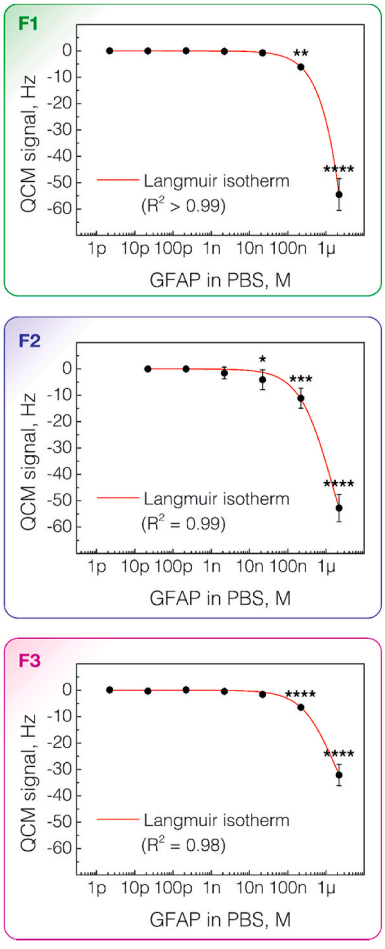

Fig. 2. Evaluation of the functionalization performance in a clean buffer. F1, F2, and F3 are the PEG-based, protein-G based, and split-antibody functionalization, respectively. For each functionalization, the mean of 3 QCM sensor signal is reported. Error bars are the SD. ANOVA (Bonferroni post-hoc) test was used against the low-concentration (≤230 pM) measurements.

2. Materials and methods

2.1. Quartz-crystal-microbalance

All the materials and reagents were purchased from Merck (Darmstadt, Germany) if not otherwise stated. The QCM is an E4 Q-Sense instrument (Biolin Scientific, Goteborg, Sweden) connected to a peristaltic pump (Ismatec, Wertheim, Germany) through Teflon tubes (Saint Gobain, Courbevoie, France). 5-MHz gold-coated AT-cut quartz sensors were used. The QCM was connected to a computer where the QSoft software acquired the real-time data from the sensors (2 s of acquisition rate). Every sensor was placed inside a chamber that contained a sample volume of about 200 μl. Frequency shifts of seven harmonics were recorded at the same time, the 5th or the 7th were used for the analysis. In every biosensing experiment 3 sensors where contemporary used, then the average shift and standard deviation (SD) were calculated. The frequency shifts were obtained by averaging the QCM signal over ≈5 min in the steady-state, always in phosphate buffer saline (PBS) 1 × . Drift, where present, was corrected by subtracting a straight baseline from the low-concentration samples not visible by the QCM (<10 nM). After every experiment, the sensors were cleaned following this procedure: plasma oxygen (Diener Femto, Germany) treatment at 100 W for 5 min; 5 min in a 5:1:1 mixture of milliQ water, ammonia (25%), and hydrogen peroxide (30%) heated at 75 °C; rinsing in milliQ water and ethanol; drying with nitrogen gas.

2.2. Surface-acoustic-wave lab-on-chip

The LoC fabrication process is here briefly described. For further details refer to (M. Agostini et al., 2019). The process consists of SAW-resonator and waveguide (WG) fabrication and polydimethylsiloxane (PDMS) microchannel bonding. The 128° X-rotated Y-cut lithium niobate (LN) wafers (Roditi International Ltd.) were diced in single substrates (2 cm × 2 cm) and cleaned in acetone (ACE), isopropanol (IPA), and O_2 plasma (Diener Femto, Germany) at 100 W for 5 min. The substrates were metalized in a thermal evaporator (Kurt J. Lesker, Nano 32) with 15 nm of Ti as an adhesion layer and 150 nm of Au. The AR-300-80 (ALLRESIST GmbH) adhesion promoter was spun onto the metalized substrates at 4000 rpm for 1 min and baked at 110 °C for 5.5 min. Negative electron-beam resist (ma-N 2403, MicroChem GmbH) was then spun at 3000 rpm for 1 min and baked at 90 °C for 1 min. The coated substrates subsequently underwent electron beam lithography (EBL) in a modified scanning electron microscope (SEM) (UltraPlus, Zeiss, with Raith GmbH lithography system), with an average area dose of 20 μC/cm^2. The resonator geometry is described in detail in (Agostini et al., 2018): the designed resonance frequency of the device was ~1 GHz, corresponding to a SAW wavelength of 4 μm. Next, Au was etched with Ar sputtering for 9 min at 3.96 mBar, using a reactive ion etching (RIE) machine (RIE Sistec, Perugia, Italy). The remaining Ti layer was finally etched in HF:H_2O (1:80) solution for 40 s. To correct for the differences among the chip sensitivities that normally arise from small variations in the fabrication outcome, the resonance frequency shift was normalized. The resonance frequency shifts of the biosensing experiments were calculated as $\delta f/|\delta f_{max}|$, where $\delta f$is the resonance frequency shift between the blank sample after the functionalization (buffer) and $\delta f_{max}$is the maximum resonance frequency shift recorded for that chip. The fabricated LoC was then mounted on a printed circuit board (PCB), wire bonded, and finally, the PDMS (Sylgard 184) microchannel was attached on its surface. The molds were made in UV-exposed negative photoresist (SU8-2100, MicroChem), 350 μm thick, on silicon wafers. The microchannels were fabricated in PDMS by standard soft-lithography and then covalently bonded on the chip by using the epoxy-mediated procedure of (Matteo Agostini et al., 2019). In this work, two LoC were fabricated and used: one for the clean-buffer set of experiments and the other for the serum-matrix set of experiments.

The LoC under test was connected to a vectorial network analyzer (VNA) (Agilent Technologies, E5071C) and a radiofrequency (RF) switch (Agilent Technologies, MSO6054A). The VNA and RF-switch communicated with a LabView® custom software through Ethernet, for acquisition timing and further data processing. The signal was averaged for 5 min after 10 min of drying in nitrogen, following the biomolecule incubation and repeated DI-water washings.

2.3. Recombinant GFAP

The GFAP protein was produced from the BL21 *E. coli* strain. Briefly, BL21 bacterial cells were transformed with pET28c (+) plasmid vector in which we cloned the human sequence of GFAP with a C-terminal tag of six histidines. A large-scale culture was prepared and protein expression was induced with Isopropyl-β-D-1-tiogalattopiranoside (IPTG) overnight at 16 °C under vigorous shaking. GFAP expressed in bacterial cells is mainly stored inside inclusion bodies. For this reason, the purification was carried out in a two-step process: first, we purified the protein in the cytoplasm; then we extracted all the GFAP from inclusion bodies. A pellet of cells was obtained by centrifugation and then resuspended in a lysis buffer. Next, the solution was sonicated on ice for 5 min at 80% of power, and DNAse, $MgCl_2$, and TritonX-100 were added to the solution to completely disrupt cell membranes, for 1 h under stirring. The suspension was centrifuged, the supernatant was kept in ice, and the pellet was used for the second step of purification. The extraction from inclusion bodies was performed following the same step used above but using buffers supplemented with a solution of urea 5 M. After centrifugation, the pellet was discarded and the solution was dialyzed to remove urea. Both supernatants with the extracted protein were purified using a Ni-NTA affinity resin (Qiagen) following manufacturing instructions. Purified protein was loaded on a polyacrylamide gel and stained with Coomassie to check if the production and purification were correctly performed. Finally, GFAP was quantified and stored at −80 °C until use. Quantification was performed on the final concentrated solution of GFAP by measuring the absorbance at 280 nm.

2.4. Functionalizations and biosensing experiment

The sensors, QCM or LoC, followed the same functionalization procedures. The surface functionalizations and the following experiments were all performed inside the instruments (QCM or LoC) by pumping the solutions through the tubing. Every concentration was incubated for 1 h before rinsing with buffer solution. For the F1 functionalization the sensors followed a two-steps process: i. treatment with streptavidin-polyethylene-glycol (2 kDa)-thiol (sPEG) (NANOCS, New York, USA) 18 μM in PBS; ii. treatment with the biotinylated anti-GFAP (b-anti-GFAP) (173211BT, Synaptic Systems, Gottingen, Germany) 60 nM in PBS. For the F2 functionalization: i. treatment with thiol-protein-G (prG) (Protein Mods, Wisconsin, USA) 90 μM in PBS; ii. treatment with the pristine anti-GFAP (antiGFAP) (166481, Santa Cruz, Texas, USA) 100 nM in PBS. For the F3 functionalization, the antibody of F2 was incubated with 5 mM of tris(2-carboxyethyl)phosphine hydrochloride (TCEP) in PBS directly into the sensor chamber. For the clean-buffer experiments, GFAP was dissolved in PBS at 2.3 pM, 23 pM, 230 pM, 2.3 nM, 23 nM, 230 nM and 2.3 μM. With serum-matrix, we refer to fetal bovine serum (FBS) in case of QCM experiments, or bovine serum albumin (BSA) at serum concentration (dissolved in PBS at 40 mg/ml) in case of UHF-SAW LoC. The sensing baseline was obtained by incubating the blank sample, which was the solution in which the analyte was dissolved. For the LoC experiments, a reference resonator was always monitored during the acquisition to subtract environmental and instrumental instabilities.

3. Results and discussion

3.1. Functionalization strategies

We explored three different functionalization strategies for detecting GFAP, as illustrated in Fig. 1. These strategies were chosen among the most used in the biosensing field. Each of them focused on a particular aspect of the biosensing process: antifouling, antibody orientation, and probe surface density. The first strategy (F1) comprised a layer of sPEG, onto which the b-antiGFAP was immobilized by the biotin-streptavidin binding. With the presence of the PEG layer, F1 assured optimal antifouling properties (Lowe et al., 2015). PEG also allowed a certain degree of freedom for antibody motion, which is expected to improve the probability of antibody-antigen interaction (Zhao and Matsui, 2007). The second strategy (F2) was based on the prG layer for the

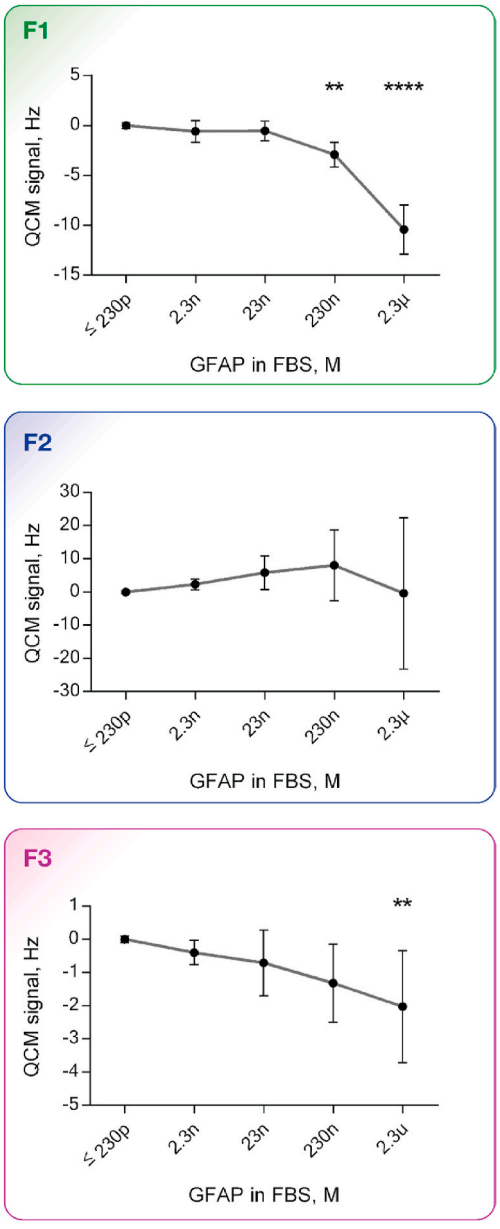

Fig. 3. Evaluation of the functionalization performance in serum-matrix. F1, F2, and F3 are the PEG-based, protein-G based, and split-antibody functionalization, respectively. For each functionalization, the mean of 3 QCM sensor signal is reported. Error bars are the SD. ANOVA (Bonferroni post-hoc) test was used against the low-concentration (≤230 pM) measurements.

Table 1
Summary of the detection performance of the three functionalization strategies evaluated by QCM.

	Clean-buffer		Serum-matrix	
	LSC	Signal @ 2.3 μM	LSC	Signal @ 2.3 μM
F1	230 nM	−54 Hz	230 nM	−10 Hz
F2	23 nM	−53 Hz	/	0 Hz
F3	230 nM	−32 Hz	2.3 μM	−2 Hz

immobilization of a pristine anti-GFAP antibody. Protein-G binds the constant fragment of the antibody (Vaisocherová et al., 2015), therefore blocking its orientation towards the solution to be analyzed. The third strategy (F3) took advantage of an h-antiGFAP immobilization on the sensor surface. By reducing the thiol-bridges naturally present in the antibody structure, we could create a highly-packed molecular layer directly on top of the sensor surface. Indeed, owing to the absence of other surface-immobilized molecules or proteins than the antibody fragments, this technique was expected to produce a sensing layer with a high-density of probes (Sharma and Mutharasan, 2013). With these three strategies, we covered the key aspects of the detection process. We tested their capability of detecting GFAP in clean buffers and in presence of biological noise (serum-matrix). We then chose the best-performing functionalization and demonstrated its use for detecting a clinically relevant concentration of GFAP with the UHF-SAW LoC.

3.2. Functionalization characterization and selection

To assess the performance in GFAP detection in terms of limit-of-detection and selectivity of the three different functionalization strategies (Fig. 1), we compared their performance by quartz-crystal-microbalance (QCM) experiments. To this end, GFAP at increasing concentrations was tested in clean buffers (PBS) and serum-matrix (FBS). The experiments were performed with gold-plated, 5-MHz fundamental frequency, QCM sensors. First, we verified the functionalization protocols by following their kinetics with real-time QCM acquisitions. Fig. 1 shows the sensorgrams obtained during the functionalization in the F1, F2, and F3 cases. Each case reveals a red-shift of the resonance frequency following the expected trend for an effective molecule immobilization. F1 and F2 show a two-step process, which corresponds to the injection and further binding of sPEG and b-antiGFAP (F1), and prG and pristine anti-GFAP (F2). F3 shows a single decreasing trend corresponding to the immobilization of the h-antiGFAP.

Following the functionalization, GFAP dissolved in PBS at 2.3 pM, 23 pM, 230 pM, 2.3 nM, 23 nM, 230 nM, and 2.3 μM was injected on sensors. The experiment results in a clean buffer are shown in Fig. 2. Here, the steady-state resonance frequency shifts after GFAP incubation and further rinsing with PBS are shown. The net shifts are a direct measurement of the amount of protein captured by the probing layer. These data were fitted with the common Langmuir isotherm (Limousin et al., 2007). Functionalized QCM sensors could detect GFAP concentrations starting from few tens of nM. These values might be ascribed by instrumental QCM sensitivity limitations and not constitute a limit determined by the probe layers (Agostini et al., 2018; De Simoni et al., 2015). The differences between the functionalizations are highlighted by the lowest significant concentration (LSC) detected and by the intensity of the signal at the maximum GFAP concentration (2.3 μM). In terms of LSC, F2 was the best-performing, with a value of 23 nM. The signal at 2.3 μM was similar for F1 and F2 (−54 Hz and −53 Hz respectively) and lower for F3 (−32 Hz). In light of this, F2 was the best performing functionalization in clean-buffers, followed by F1 and F3. Using the Sauerbrey equation (Vogt et al., 2004), it is possible to estimate the surface density of the molecules on the sensor plates. At the end of the functionalization procedure, the surface mass density of F1, F2, and F3 was 1093 ng/cm^2, 5807 ng/cm^2, and 2063 ng/cm^2, respectively.

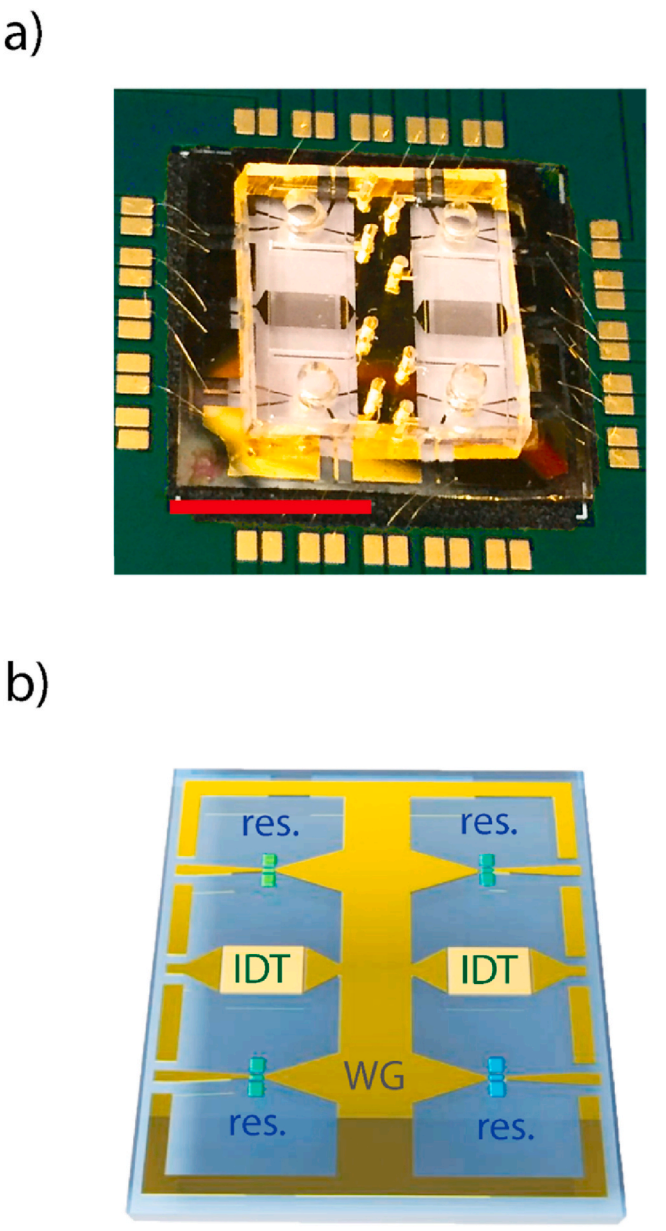

Fig. 4. Full-SAW biochip. a) Photo of a mounted device. Scale bar is 1 cm. b) Simplified illustration of the biochip, composed by an LN substrate, WGs, resonator-sensors, and mixing IDTs. The PDMS microfluidic channel is not shown for clarity of visualization.

Since streptavidin has four binding sites for the biotin linked to the constant fragment of the anti-GFAP, the estimated surface density of paratopes for F1, F2, and F3 are 2.1×10^{13}paratopes/cm^2, 8.6×10^{13}paratopes/cm^2, and 4.5×10^{13}paratopes/cm^2. It emerges that the best performing functionalization in clean-buffer (F2) is the one that exhibits the highest paratope density on the sensor surface. As a remark, F2 is based on a thiolated protein-G, ensuring also the correct orientation of the antibodies towards the solution with GFAP. Even though the paratopes density of F3 is higher than F1, the F1 functionalization could detect GFAP better than F3, probably owing to the increased mobility of the antibody provided by the PEG chain (Zhao and Matsui, 2007). Therefore, the optimal detection process in clean-buffer appears to be a trade-off between the paratope surface density, and the antibody mobility with correct orientation.

We then proceeded to test the functionalizations in presence of bio-noise, namely by dissolving GFAP in a serum-matrix (FBS). The results

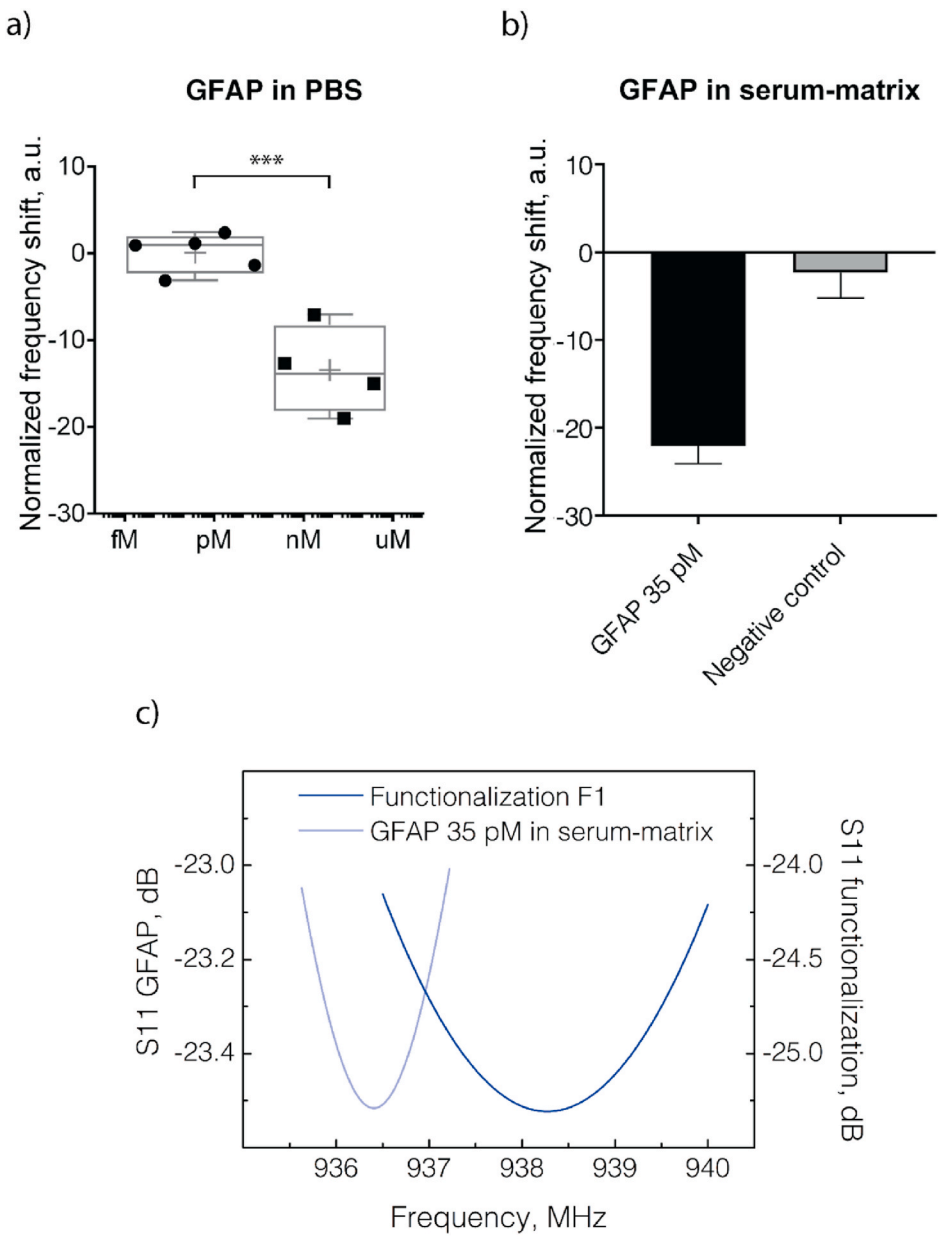

Fig. 5. GFAP detection with the UHF-SAW LoC. a) Experiments with GFAP in PBS at several concentrations. *t*-test with 23 pM as grouping threshold $P < 0.001$. b) Experiments with GFAP in serum-matrix, error bars are the SD of the signal resulting from repeated sensor washings. c) Reflected power spectrum (S11) of the resonator showing the resonance shift in the F1 and GFAP in the serum-matrix case.

are shown in Fig. 3. Here, F1 and F3 could significantly discriminate GFAP concentrations to the FBS baseline value. F1 reported similar detection characteristics to the PBS case, except for a reduction of the signal at the maximum concentration. While F3 suffered from a higher deterioration of the detection performance, F2 was strongly affected by non-specific binding of other proteins, which hindered the possibility of detecting any GFAP concentration in serum-matrix.

Table 1 summarizes the GFAP detection performance obtained with the three functionalizations tested by QCM. All three functionalizations were effective in clean buffers, but only F1 and F3 could also significantly detect at least one concentration of GFAP in presence of FBS as a buffer. Among these, F1 was the best performing both in terms of LSC and specificity. FBS is the liquid fraction of clotted blood from fetal calves, depleted of cells, fibrin, and clotting factors. FBS contains a variety of small molecules like amino acids, sugars, lipids, and hormones, but bovine serum albumin (BSA) is its major component, present at several mg/ml (Soutar et al., 2019). We can, therefore, estimate the functionalization specificities to GFAP against BSA as ≈1/180 molecules for F1, and ≈1/18 molecules for F3. These experiments show that, in the presence of bio-noise (i.e., in serum-matrix), the use of a PEG-based linker can result in outperforming probing layers to protein-G and reduced antibody strategies. This can be attributed to the antifouling effect of PEG combined with its flexibility which is expected to improve the probability of antibody-antigen interaction (see Sec. 3.1). In light of the previous estimation of the paratope density, the results in presence of bio-noise highlight another key aspect of the detection: the antifouling properties of the functionalization. The capability of F2 to immobilize a large number of paratopes is not enough to ensure high detection performance of GFAP in serum-matrix. The PEG-based functionalization (F1), and the split-antibody functionalization (F2) to less extent, outperform F2 and provide significant signals also in presence of bio-noise. As a result, when the detection process is performed in buffers

similar to one of the real samples, the ideal functionalization appears to be a three-way optimization problem between the molecules' surface density, mobility/orientation, and antifouling properties.

3.3. Biomarker detection with the surface-acoustic-wave resonator biosensor

Table 1 shows that our QCM setup could not detect GFAP concentrations below a few tens of nM even in clean buffers. The GFAP concentration to be revealed, relevant for clinical applications, is in the range of few fM up to the nM level. This is the case of several pathologies, such as GBM (Jung et al., 2007; Tichy et al., 2016) and TBIs (Frankel et al., 2019; Nylén et al., 2006; Vos et al., 2004; Yue et al., 2019). The detection limit can be improved by adding a signal amplification step, as, for example, labeling analytes with heavy tags (e.g., nanoparticles) for increasing mass loading on QCM sensors (Ding et al., 2013; Masdor et al., 2016). However, label-free techniques are preferable when priorities are ease of implementation and cost reduction, such as in the case of PoC diagnostics.

In the last few years, we developed an capable of manipulating fluids and detecting sub-nM concentrations of proteins without signal amplification and labeling (Agostini et al., 2018; M. Agostini et al., 2019). This device, being miniaturized, fabricated with highly parallelizable processes, passive, with electrical-readout, is an ideal platform for the realization of a PoC instrument for GFAP detection. The ultrasensitive full-SAW LoC biochip is shown in Fig. 4. The LoC can be described as the combination of four levels (bottom-up): substrate, waveguide (WG), resonator-biosensors, and mixing IDTs, microfluidic layer. The substrate and the single resonator design were the same as the ones presented in our previous works (Agostini et al., 2018; M. Agostini et al., 2019), with a resonance frequency at ~1 GHz. Resonators act as gravimetric sensors. Starting from the bottom layer of Fig. 4b, the substrate was an LN crystal, on top of which a coplanar WG was designed to have 50 Ω resistance for impedance matching. The third layer contained the resonators and IDTs for mixing. Four 2-port SAW resonators with positive and negative reflectors (PNRs) and two bidirectional single-finger IDTs (~50 MHz) were patterned and individually connected to the WG. Lastly, the topmost layer was the PDMS microchannel: it comprised four independent microchambers with inlets-outlets for liquid sample handling and two air-filled microchambers on top of the IDTs for avoiding SAW damping. The device was finally mounted and wire-bonded on a PCB. This LoC was designed such that four multiplexed measurements were feasible–one for each sensor and microchamber–while liquid mixing could be realized by activating the two low-frequency IDTs. A reference resonator was always recorded during the experiments and subtracted from the functionalized sensor signal. This allowed for the removal of noise stemming from environmental and instrumental instabilities. Similarly to what was carried out with the QCM, this UHF-SAW LoC was functionalized with the F1 probing layer and tested with several GFAP concentrations in different conditions. Fig. 5 shows the resonance frequency shifts of the resonator biosensors upon exposure to different GFAP concentrations. By dissolving GFAP in a clean buffer, the two distributions of Fig. 5a become significantly separated, minimizing the P-value, for a GFAP concentration threshold of 23 pM. This value, if compared with the LSC of the QCM experiments, reveals a 3-orders-of-magnitude increase of the detection performance in terms of limit of detection. To assess the specificity of this device, we repeated the same experiment with GFAP dissolved at 35 pM in BSA at serum-concentration (40 mg/ml). The results are shown in Fig. 5b and c. The full-SAW LoC could detect the GFAP biomarker also in this case, showing a normalized signal ~1 order of magnitude larger than the negative control. The resonance-frequency shift of the serum-matrix experiment is reported in Fig. 5c. The net shift between the F1-functionalization and GFAP cases is ~1.7 MHz.

4. Conclusion

In this work, we designed and tested three different functionalization strategies for GFAP biomarker detection. These strategies were chosen among the most used in the biosensing field and never previously compared within the same experimental frame. The first (F1) was based on a PEG-chain for antifouling, the second (F2) on a protein-G linker for antibody-orientation, and the third (F3) on antibody-splitting and direct surface immobilization for high-surface coverage. We tested their capability of detecting GFAP in clean buffers and in presence of bio-noise (serum-matrix) with gold QCM sensors. We then chose the best-performing functionalization, F1, and demonstrated its use with the UHF-SAW LoC. The LoC here used exploited ~1 GHz SAW resonators as ultrasensitive mass-sensors, and a microfluidic network for precise fluid routing. GFAP was significantly detected at clinically-relevant concentrations both in clean-buffers (>23 pM) and in serum-matrix (35 pM). As a comparison with previous works, Arya et al. (2013) and Wang et al. (Wang, 2017) proposed electrochemical sensors for GFAP detection in clean-buffers. The first work showed a limit of detection (LoD) of a few tens of fM, while the second of hundreds of pM. J. Song et al. (2017) detected few tens of pM of GFAP in clean-buffers by using an organic-field-effect-transistor (OFET) with polyethylene glycol (PEG) based functionalization. To the best of our knowledge, the only paper showing a device for the detection of GFAP in serum-matrix was published by Y. Ma et al. (2018). The authors, exploiting fluorescently labeled GFAP, reached an LoD of the order of pM. The UHF-SAW LoC here presented, combined with the non-labeling detection technique developed, showed clinically relevant results on the GFAP detection in serum-matrix. The device can be further developed and engineered with the aim of realizing a point-of-care biosensing platform for the detection of multiple brain-pathology biomarkers in serum or whole blood. In the light of this biosensing performance and the advantages of an all-electrical readout, this LoC has the potential to be further developed for other, non-CNS, relevant pathologies, where a PoC diagnosis could be a breakthrough, such as a virus and bacteria detection.

CRediT authorship contribution statement

M. Agostini: Conceptualization, Formal analysis, Investigation, Writing - original draft, Writing - review & editing. **F. Amato:** Investigation, Writing - review & editing. **M.L. Vieri:** Investigation, Writing - review & editing. **G. Greco:** Investigation, Writing - review & editing. **I. Tonazzini:** Investigation, Writing - review & editing. **L. Baroncelli:** Investigation, Supervision, Writing - review & editing. **M. Caleo:** Supervision, Writing - review & editing. **E. Vannini:** Investigation, Writing - review & editing. **M. Santi:** Investigation, Writing - review & editing. **G. Signore:** Supervision, Writing - review & editing. **M. Cecchini:** Conceptualization, Formal analysis, Funding acquisition, Supervision, Writing - review & editing.

Declaration of competing interest

The authors declare that they have no known competing financial interests or personal relationships that could have appeared to influence the work reported in this paper.

References

Abdelhak, A., Huss, A., Kassubek, J., Tumani, H., Otto, M., 2018. Serum GFAP as a biomarker for disease severity in multiple sclerosis. Sci. Rep. 8, 1–7. https://doi.org/10.1038/s41598-018-33158-8.

Agostini, M., Greco, G., Cecchini, M., 2019. Full-SAW microfluidics-based lab-on-a-chip for biosensing. IEEE Access 7, 70901–70909. https://doi.org/10.1109/ACCESS.2019.2919000.

Agostini, Matteo, Greco, G., Cecchini, M., 2019. Polydimethylsiloxane (PDMS) irreversible bonding to untreated plastics and metals for microfluidics applications. Apl. Mater. 7 https://doi.org/10.1063/1.5070136.

Agostini, M., Greco, G., Cecchini, M., 2018. A Rayleigh surface acoustic wave (R-SAW) resonator biosensor based on positive and negative reflectors with sub-nanomolar limit of detection. Sensor. Actuator. B Chem. 254, 1–7. https://doi.org/10.1016/j.snb.2017.07.014.

Arya, S.K., Pui, T.S., Wong, C.C., Kumar, S., Rahman, A.R.A., 2013. Effects of the electrode size and modification protocol on a label-free electrochemical biosensor. Langmuir 29, 6770–6777. https://doi.org/10.1021/la401109r.

Axelsson, M., Malmeström, C., Nilsson, S., Haghighi, S., Rosengren, L., Lycke, J., 2011. Glial fibrillary acidic protein: a potential biomarker for progression in multiple sclerosis. J. Neurol. 258, 882–888. https://doi.org/10.1007/s00415-010-5863-2.

Cecchini, M., Girardo, S., Pisignano, D., Cingolani, R., Beltram, F., 2008. Acoustic-counterflow microfluidics by surface acoustic waves. Appl. Phys. Lett. 92, 104103. https://doi.org/10.1063/1.2889951.

De Simoni, G., Signore, G., Agostini, M., Beltram, F., Piazza, V., 2015. A surface-acoustic-wave-based cantilever bio-sensor. Biosens. Bioelectron. 68, 570–576. https://doi.org/10.1016/j.bios.2014.12.058.

Destgeer, G., Sung, H.J., 2015. Recent advances in microfluidic actuation and micro-object manipulation via surface acoustic waves. Lab Chip 15, 2722–2738. https://doi.org/10.1039/C5LC00265F.

Ding, P., Liu, R., Liu, S., Mao, X., Hu, R., Li, G., 2013. Reusable gold nanoparticle enhanced QCM immunosensor for detecting C-reactive protein. Sensor. Actuator. B Chem. 188, 1277–1283. https://doi.org/10.1016/j.snb.2013.07.099.

Franke, T., Abate, A.R., Weitz, D.A., Wixforth, A., 2009. Surface acoustic wave (SAW) directed droplet flow in microfluidics for PDMS devices. Lab Chip 9, 2625–2627. https://doi.org/10.1039/b906819h.

Frankel, M., Fan, L., Yeatts, S.D., Jeromin, A., Vos, P.E., Wagner, A.K., Wolf, B.J., Pauls, Q., Lunney, M., Merck, L.H., Hall, C.L., Palesch, Y., Silbergleit, R., David, W., 2019. The association of very early serum levels of S100B, GFAP, UCH-L1, and SBDP with outcome in ProTECT III. J. Neurotrauma 1–32. https://doi.org/10.1089/neu.2018.5809.

Friend, J.R., Yeo, L.Y., 2011. Microscale acoustofluidics: microfluidics driven via acoustics and ultrasonics. Rev. Mod. Phys. 83, 647–704. https://doi.org/10.1103/RevModPhys.83.647.

Greco, G., Agostini, M., Barone, S., Cecchini, M., 2017a. Embryo development in dynamic microfluidic systems. Sensor. Actuator. B Chem. 250, 525–532. https://doi.org/10.1016/j.snb.2017.04.186.

Greco, G., Agostini, M., Shilton, R., Travagliati, M., Signore, G., Cecchini, M., 2017b. Surface acoustic wave (SAW)-Enhanced chemical functionalization of gold films. Sensors 17, 2452. https://doi.org/10.3390/s17112452.

Greco, G., Agostini, M., Tonazzini, I., Sallemi, D., Barone, S., Cecchini, M., 2018. Surface-acoustic-wave (SAW)-Driven device for dynamic cell cultures. Anal. Chem. 90, 7450–7457. https://doi.org/10.1021/acs.analchem.8b00972.

Humphreys, I., Wood, R.L., Phillips, C.J., Macey, S., 2013. The costs of traumatic brain injury: a literature review. Clin. Outcomes Res. 5–281. https://doi.org/10.2147/CEOR.S44625.

Jung, C.S., Foerch, C., Schänzer, A., Heck, A., Plate, K.H., Seifert, V., Steinmetz, H., Raabe, A., Sitzer, M., 2007. Serum GFAP is a diagnostic marker for glioblastoma multiforme. Brain 130, 3336–3341. https://doi.org/10.1093/brain/awm263.

Limousin, G., Gaudet, J.P., Charlet, L., Szenknect, S., Barthès, V., Krimissa, M., 2007. Sorption isotherms: a review on physical bases, modeling and measurement. Appl. Geochem. 22, 249–275. https://doi.org/10.1016/j.apgeochem.2006.09.010.

Lowe, S., O'Brien-Simpson, N.M., Connal, L.A., 2015. Antibiofouling polymer interfaces: poly(ethylene glycol) and other promising candidates. Polym. Chem. 6, 198–212. https://doi.org/10.1039/c4py01356e.

Ma, Yunsu, Xu, G., Wei, F., Cen, Y., Song, Y., Ma, Yujie, Xu, X., Shi, M., Sohail, M., Hu, Q., 2018. Carbon dots based immunosorbent assay for the determination of GFAP in human serum. Nanotechnology 29. https://doi.org/10.1088/1361-6528/aaabea.

Masdor, N.A., Altintas, Z., Tothill, I.E., 2016. Sensitive detection of Campylobacter jejuni using nanoparticles enhanced QCM sensor. Biosens. Bioelectron. 78, 328–336. https://doi.org/10.1016/j.bios.2015.11.033.

Nylén, K., Öst, M., Csajbok, L.Z., Nilsson, I., Blennow, K., Nellgård, B., Rosengren, L., 2006. Increased serum-GFAP in patients with severe traumatic brain injury is related to outcome. J. Neurol. Sci. 240, 85–91. https://doi.org/10.1016/j.jns.2005.09.007.

Preston, A.N., Cervasio, D.A., Laughlin, S.T., 2019. Visualizing the brain's astrocytes. Methods Enzymol. 622, 129–151. https://doi.org/10.1016/bs.mie.2019.02.006. Visualizing.

Sharma, H., Mutharasan, R., 2013. Half antibody fragments improve biosensor sensitivity without loss of selectivity. Anal. Chem. 85, 2472–2477. https://doi.org/10.1021/ac3035426.

Shilton, R.J., Mattoli, V., Travagliati, M., Agostini, M., Desii, A., Beltram, F., Cecchini, M., 2015. Rapid and controllable digital microfluidic heating by surface acoustic waves. Adv. Funct. Mater. 25 https://doi.org/10.1002/adfm.201501130.

Shilton, R.J., Travagliati, M., Beltram, F., Cecchini, M., 2014. Nanoliter-droplet acoustic streaming via ultra high frequency surface acoustic waves. Adv. Mater. 26, 4941–4946. https://doi.org/10.1002/adma.201400091.

Song, J., Dailey, J., Li, H., Jang, H.J., Zhang, P., Wang, J.T.H., Everett, A.D., Katz, H.E., 2017. Extended solution gate OFET-based biosensor for label-free glial fibrillary acidic protein detection with polyethylene glycol-containing bioreceptor layer. Adv. Funct. Mater. 27 https://doi.org/10.1002/adfm.201606506.

Soutar, M.P.M., Kempthorne, L., Annuario, E., Luft, C., Wray, S., Ketteler, R., Ludtmann, M.H.R., Plun-Favreau, H., 2019. FBS/BSA media concentration determines CCCP's ability to depolarize mitochondria and activate PINK1-PRKN mitophagy. Autophagy 15, 2002–2011. https://doi.org/10.1080/15548627.2019.1603549.

Takano, R., Misu, T., Takahashi, T., Sato, S., Fujihara, K., Itoyama, Y., 2010. Astrocytic damage is far more severe than demyelination in NMO: a clinical CSF biomarker study. Neurology 75, 208–216. https://doi.org/10.1212/WNL.0b013e3181e2414b.

Taylor, C.A., Bell, J.M., Breiding, M.J., Xu, L., 2017. Traumatic brain injury–related emergency department visits, hospitalizations, and deaths — United States, 2007 and 2013. MMWR Surveillance Summaries 66, 1–16. https://doi.org/10.15585/mmwr.ss6609a1.

Tichy, J., Spechtmeyer, S., Mittelbronn, M., Hattingen, E., Rieger, J., Senft, C., Foerch, C., 2016. Prospective evaluation of serum glial fibrillary acidic protein (GFAP) as a diagnostic marker for glioblastoma. J. Neuro Oncol. 126, 361–369. https://doi.org/10.1007/s11060-015-1978-8.

Travagliati, M., De Simoni, G., Lazzarini, C., Piazza, V., Beltram, F., Cecchini, M., 2012. Interaction-free, automatic, on-chip fluid routing by surface acoustic waves. Lab Chip 12, 2621–2624. https://doi.org/10.1039/c2lc40396j.

Travagliati, M., Shilton, R.J., Pagliazzi, M., Tonazzini, I., Beltram, F., Cecchini, M., 2014. Acoustofluidics and whole-blood manipulation in surface acoustic wave counterflow devices. Anal. Chem. 86, 10633–10638. https://doi.org/10.1021/ac502465s.

UniProt database, 2020. WWW Document. https://www.uniprot.org/uniprot/P14136.

Vaisocherová, H., Brynda, E., Homola, J., 2015. Functionalizable low-fouling coatings for label-free biosensing in complex biological media: advances and applications. Anal. Bioanal. Chem. 407, 3927–3953. https://doi.org/10.1007/s00216-015-8606-5.

Vogt, B.D., Lin, E.K., Wu, W.I., White, C.C., 2004. Effect of film thickness on the validity of the sauerbrey equation for hydrated polyelectrolyte films. J. Phys. Chem. B 108, 12685–12690. https://doi.org/10.1021/jp0481005.

Vos, P.E., Lamers, K.J.B., Hendriks, J.C.M., Van Haaren, M., Beems, T., Zimmerman, C., Van Geel, W., De Reus, H., Biert, J., Verbeek, M.M., 2004. Glial and neuronal proteins in serum predict outcome after severe traumatic brain injury. Neurology 62, 1303–1310. https://doi.org/10.1212/01.WNL.0000120550.00643.DC.

Wang, T., 2017. Electrochemical quantitative detection of glial fibrillary acidic protein based on molecularly imprinted polymer sensor. International Journal of Electrochemical Science 12, 7341–7350. https://doi.org/10.20964/2017.08.69.

Wang, K K, Yang, Z, Zhu, T, Shi, Y, Rubenstein, R, Tyndall, J A, Manley, G T, 2018. An update on diagnostic and prognostic biomarkers for traumatic brain injury. Expert Rev. Mol. Diagn. 18, 165–180.

Yue, J.K., Yuh, E.L., Korley, F.K., Winkler, E.A., Sun, X., Puffer, R.C., Deng, H., Choy, W., Chandra, A., Taylor, S.R., Ferguson, A.R., Huie, J.R., Rabinowitz, M., Puccio, A.M., Mukherjee, P., Vassar, M.J., Wang, K.K.W., Diaz-Arrastia, R., Okonkwo, D.O., Jain, S., Manley, G.T., Adeoye, O.M., Badjatia, N., Boase, K., Bodien, Y.G., Bullock, M.R., Chesnut, R.M., Corrigan, J.D., Crawford, K., Dikmen, S.S., Duhaime, A.-C., Ellenbogen, R.G., Feeser, V., Foreman, B., Gardner, R.C., Gaudette, E., Giacino, J.T., Goldman, D.P., Gonzalez, L., Gopinath, S., Gullapalli, R., Hemphill, J.C., Hotz, G., Kramer, J.H., Kreitzer, N.P., Levin, H.S., Lindsell, C.J., Machamer, J., Madden, C.J., Martin, A.J., McAllister, T.W., McCrea, M., Merchant, R., Nelson, L.D., Noel, F., Palacios, E.M., Perl, D.P., Puccio, A.M., Rabinowitz, M., Robertson, C.S., Rosand, J., Sander, A.M., Satris, G.G., Schnyer, D. M., Seabury, S.A., Sherer, M., Stein, M.B., Temkin, N.R., Toga, A.W., Valadka, A.B., Vassar, M.J., Vespa, P.M., Yuh, E.L., Zafonte, R., 2019. Association between plasma GFAP concentrations and MRI abnormalities in patients with CT-negative traumatic brain injury in the TRACK-TBI cohort: a prospective multicentre study. Lancet Neurol. 18, 953–961. https://doi.org/10.1016/s1474-4422(19)30282-0.

Zhang, J., Zhang, C.H., Lin, X.L., Zhang, Q., Wang, J., Shi, S.L., 2013. Serum glial fibrillary acidic protein as a biomarker for differentiating intracerebral hemorrhage and ischemic stroke in patients with symptoms of acute stroke: a systematic review and meta-analysis. Neurol. Sci. 34, 1887–1892. https://doi.org/10.1007/s10072-013-1541-3.

Zhao, Z., Matsui, H., 2007. Accurate immobilization of antibody-functionalized peptide nanotubes on protein-patterned arrays by optimizing their ligand-receptor interactions. Small 3, 1390–1393. https://doi.org/10.1002/smll.200700006.